

## A Trimer of Ultrafast Nanomotors: Synthesis, Photochemistry and Self-Assembly on Graphite

Arjen Cnossen,<sup>[a]</sup> Dirk Pijper,<sup>[a]</sup> Tibor Kudernac,<sup>[a, b]</sup> Michael M. Pollard,<sup>[a]</sup>  
Nathalie Katsonis,<sup>[a]</sup> and Ben L. Feringa\*<sup>[a]</sup>

Synthetic molecular motors may play an essential role in the development of nanoscale mechanical devices, as evident from the many fascinating natural systems that use nanometre-sized motors to drive crucial biological processes.<sup>[1,2]</sup> Biological motors such as the bacterial flagellar motor pose a major challenge to emulate and provide a source of inspiration that has spurred the construction of a wide range of molecular systems in which motion is controlled by chemical, electrochemical, photochemical or thermal input.<sup>[3–8]</sup> The structural modifications induced in such complex molecular systems can be observed by scanning tunnelling microscopy (STM) in chemisorbed and physisorbed monolayers,<sup>[9,10]</sup> in particular under ambient conditions.<sup>[11,12]</sup>

Our group has reported on light-driven molecular motors based on sterically overcrowded alkenes,<sup>[13]</sup> for example, compound **1**.<sup>[14]</sup> With these systems, unidirectional rotation of the upper half relative to the lower half around the central olefin (the axis of rotation) is performed through four discrete steps: two photochemical *cis–trans* isomerisations each followed by an irreversible thermal helix inversion. To be able to harness work from these systems, we envision that two key issues need to be addressed.<sup>[7,8,15]</sup> First, the rate of rotation of the motor has to be increased to a level at which it is fast enough to compete with the surrounding Brownian motion.<sup>[16,17]</sup> Second, it seems essential to take the motor molecules operating in solution, in which they possess no positional or orientational order, and graft them onto a

surface, either covalently attached or physisorbed.<sup>[11]</sup> Light-driven molecular motors have already been covalently attached to gold nanoparticles<sup>[18]</sup> and a quartz surface.<sup>[19]</sup> Another strategy to harness useful work from these systems is anticipated to be their incorporation into larger, flat molecular assemblies that are able to physisorb onto a surface.<sup>[10,20,21]</sup>

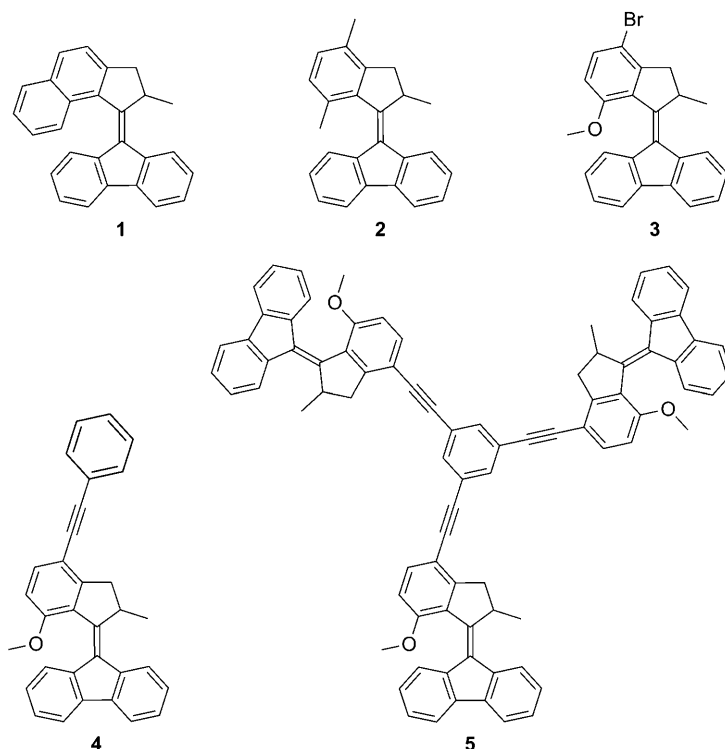
In nature, motors sometimes operate alone, such as the bacterial flagellar motor, but more commonly they act in concert to achieve a common goal, such as muscle proteins like myosin and the transport proteins kinesin and dynein.<sup>[1]</sup> Similarly, the concerted action of several synthetic molecular motors with positional ordering could make it easier to extract useful work from these systems.

Herein we report molecular motor trimer **5**, which was found to form self-assembled monolayers at the interface between the surface of highly oriented pyrolytic graphite (HOPG) and the solvent (1-phenyloctane). The structure of the stable arrays was determined by means of STM at the liquid/solid interface. Trimer **5** is based on the new light-driven molecular motor **4**, which has a greatly increased rotation speed compared with systems previously reported. Recently we described the redesign of our molecular motors, wherein the naphthalene moiety is exchanged for a substituted phenyl ring (Scheme 1, **1** and **2**).<sup>[22]</sup> The rationale for this modification was to facilitate the synthesis of functionalised motors by avoiding the need to derivatise the naphthalene moiety through multistep syntheses, as well as the possibility that changing the substituent in the fjord region would provide a new handle to tune the speed of the rate-limiting helix inversion. The design of **3** is based on second-generation molecular motor **2**. The most notable change in molecular design compared with previously described systems is the substitution of the dimethylphenyl moiety in the upper half of the motor by a methoxy-substituted phenyl group. This decreases the steric hindrance in the fjord region, which should in turn increase the rate of the rate-limiting thermal isomerisation step in the rotary cycle of **4** in comparison with parent motor **2**.

[a] A. Cnossen, D. Pijper, Dr. T. Kudernac, Dr. M. M. Pollard, Dr. N. Katsonis, Prof. B. L. Feringa  
Stratingh Institute for Chemistry, University of Groningen  
Nijenborgh 4, 9747 AG, Groningen (The Netherlands)  
Fax: (+31) 50-363-4296  
E-mail: b.l.feringa@rug.nl

[b] Dr. T. Kudernac  
Current address: Laboratory of Photochemistry and Spectroscopy  
Katholieke Universiteit Leuven Celestijnenlaan 200-F  
3001 Leuven (Belgium)

Supporting information for this article is available on the WWW under <http://dx.doi.org/10.1002/chem.200802718>.



Scheme 1. Unidirectional light-driven molecular motors based on overcrowded alkenes.

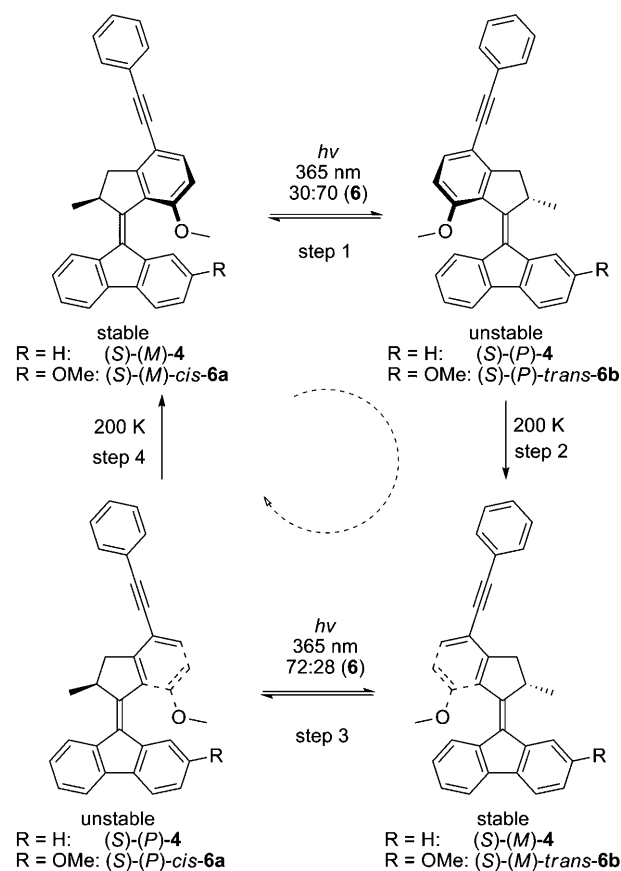
The key step in the synthesis of **3** is a Barton–Kellogg diazo–thio ketone coupling<sup>[23,24]</sup> followed by reductive desulfurisation to introduce the sterically overcrowded olefinic bond. The aryl bromide in the upper half of **3** allows for further functionalisation. Starting from **3**, both motor **4** and motor trimer **5** were synthesised in one step by Sonogashira coupling<sup>[25]</sup> with phenyl acetylene and 1,3,5-triethynylbenzene, respectively. Enantioresolution of **4** and **5** was performed with chiral stationary phase HPLC. The absolute configuration was assigned by comparison of the circular dichroism (CD) spectrum to that of parent motor **1**. The *cis* and *trans* isomers of motor **6** were separated by column chromatography, and their configuration was assigned by using <sup>1</sup>H NMR and NOE spectroscopy measurements.

First, the photochemical *cis*–*trans* isomerisation of (*S*)-(*M*)-**4** was analysed by using UV/Vis and CD spectroscopies (Scheme 2, steps 1 and 3). UV irradiation ( $\lambda_{\text{max}} = 365 \text{ nm}$ ) of an isopentane solution of (*S*)-(*M*)-**4** at 150 K lead to the formation of a new absorption at 400 nm in the UV/Vis spectrum (Figure 1). Also, the major absorptions in the CD spectrum inverted, which indicated a change in the helicity of the molecule and is consistent with the formation of thermally unstable (*S*)-(*P*)-**4**. After warming to 200 K in the dark for 30 min, the spectrum corresponding to stable (*S*)-(*M*)-**4** was regenerated. All of these observations are consistent with the UV/Vis and CD data for molecular motor **1**.<sup>[14]</sup>

The kinetic parameters of the thermal helix inversion (Scheme 2, steps 2 and 4) of motor **4** were determined by monitoring its CD absorption at  $\lambda = 218 \text{ nm}$  over time in the dark at four different temperatures ranging from 167.5 to

175 K. By using the Eyring equation, the rate constants  $k_t$  of the first-order process were used to determine the Gibbs energy of activation ( $\Delta^\ddagger G^\circ$ ) to be  $51 \text{ kJ mol}^{-1}$ . The half-life ( $t_{1/2}$ ) under standard conditions was obtained after extrapolation of the data collected at low temperature (Table 1). The thermal step of motor **4** is considerably faster than that of parent motor **1**:  $t_{1/2}$  of the unstable isomer was decreased by a factor  $10^6$ , making it capable of rotation in the microsecond regime at room temperature.<sup>[26]</sup>

As the changes in structure from **1** to **4** had an unexpectedly large effect on the speed of the thermal step, the photochemical and thermal isomerisation processes were studied to prove that motor **4** behaves similarly to parent motor **1**.

Scheme 2. Full 360° rotational cycle for symmetrical motor **4** and non-symmetrical motor **6**.

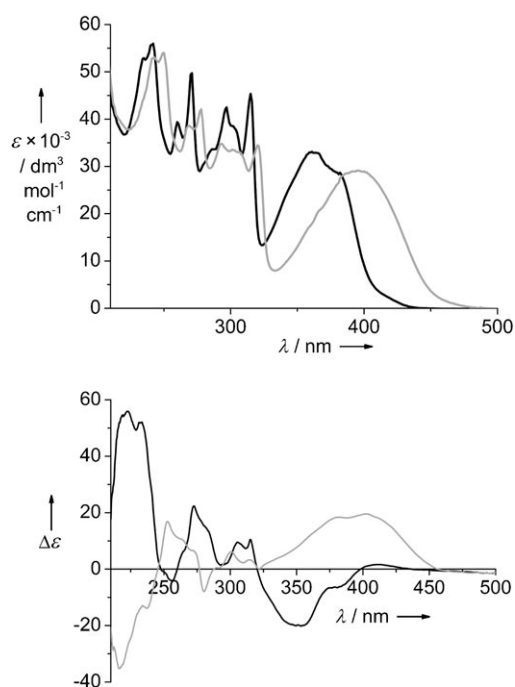


Figure 1. UV/Vis (top) and CD (bottom) spectra (isopentane, 150 K) of (2'S)-(M)-**4** (black) and the photostationary state mixture of stable (S)-(M)-**4** and unstable (S)-(P)-**4** (grey) after irradiation ( $\lambda_{\text{max}} = 365$  nm).

Table 1. Kinetic parameters of the thermal helix inversion of motors **1**, **2** and **4**.

Motor	$k$ [ $\text{s}^{-1}$ ] (20°C)	$\Delta^+G^\circ$ [ $\text{kJ mol}^{-1}$ ]	$t_{1/2}$ [s] (20°C)
<b>1</b> <sup>[a]</sup>	$3.64 \times 10^{-3}$	85	190
<b>2</b> <sup>[a]</sup>	$4.6 \times 10^{-2}$	79	15
<b>4</b> <sup>[b]</sup>	$4.3 \times 10^3$	51	$1.6 \times 10^{-4}$

[a] Solution in hexane. [b] Solution in isopentane.

Motor **4** contains a symmetrical lower half, so just one photochemical and one thermal isomerisation step convert the molecule to its initial stable isomer. To investigate if the propeller unit in **4** was still rotating unidirectionally relative to the stator unit, molecular motor **6** with an unsymmetrical lower half was synthesised. Due to the presence of the methoxy substituent in the lower half, all four states in the rotary cycle have different spectroscopic properties. The unidirectionality of the rotary cycle of motor **6** was studied by correlating the ratio of stable/unstable isomers at the PSS (isopentane, 150 K) to the ratio of *cis/trans* after the thermal isomerisation step.<sup>[27]</sup> The ratio of stable/unstable in the PSS was determined from the UV/Vis spectra after irradiation at two different wavelengths according to a method developed by Fischer.<sup>[28]</sup> Starting from stable *cis*-**6a**, a ratio of stable *cis*-**6a**/unstable *trans*-**6b** of 30:70 at the PSS in step 1 was determined. HPLC analysis of the PSS mixture after warming to room temperature also yielded a stable *cis*/stable *trans* ratio of 30:70, strongly indicating that the thermal helix inversion is unidirectional. The ratio of stable *trans*-**6b**/unstable *cis*-**6a** in step 3 was determined to be 28:72, whereas HPLC analysis of the mixture after warming to room tem-

perature gave a stable *trans*-**6b**/stable *cis*-**6a** ratio of 29:71, which provides a strong indication that the second thermal helix inversion is also unidirectional; hence, compound **6** operates as a unidirectional light-driven molecular motor.

To confirm that the motor function was preserved while in a conjugated trimeric system, the photochemical and thermal isomerisations were followed by using UV/Vis and CD spectroscopies (Figure 2). To ensure that **5** remained soluble

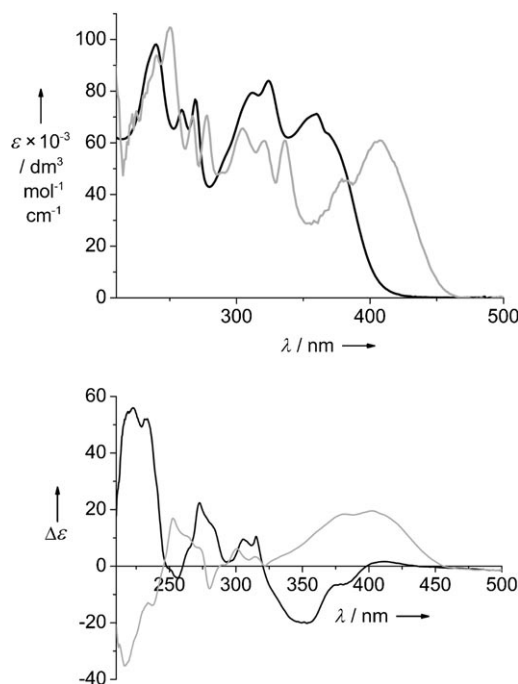


Figure 2. UV/Vis (top) and CD (bottom) spectra (isopentane/diethyl ether 1:1, 150 K) of (S)-(M)-(S')-(M')-(S'')-(M'')-**5** (black) and the PSS mixture containing (S)-(M)-(S')-(M')-(S'')-(M'')-**5** and the mixture of unstable isomers (grey) resulting from the photochemically induced *cis-trans* isomerisations upon irradiation ( $\lambda_{\text{max}} = 365$  nm).

at low temperature, a 1:1 mixture of isopentane and diethyl ether was used as the solvent. In analogy to **4**, UV irradiation ( $\lambda_{\text{max}} = 365$  nm) of trimer **5** in PSS at 150 K resulted in the appearance of a distinct absorption at around 415 nm in the UV/Vis spectrum and an inversion of the major absorption bands in the CD spectrum. Both spectra reverted to their original when the sample was allowed to warm to 200 K in the dark for 30 min. These observations indicate that the key photochemical and thermal isomerisation behaviour of the individual motor units in the trimer is preserved. Based on the quantitative spectral changes observed for the trimer compared with those observed for the monomer, we expect that the three motor units in the trimer operate independently (Figure 1 vs. Figure 2).

The self-organised monolayer formed by **5** at the HOPG/phenyloctane interface was studied by STM. After deposition of a saturated solution of enantiomerically pure (S)-(M)-(S')-(M')-(S'')-(M'')-**5** in phenyloctane on freshly cleaved HOPG, large ordered areas were observed

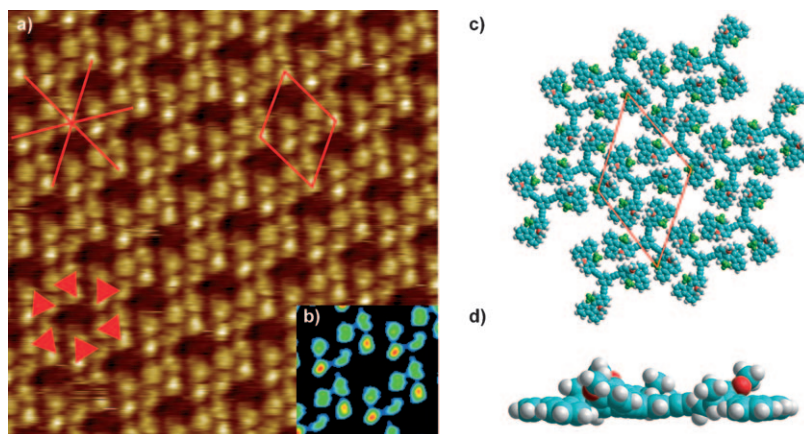


Figure 3. a) STM image of the self-assembled monolayer of enantiomerically pure  $(S)-(M)-(S')-(M')-(S'')-(M'')$ -**5** on HOPG;  $18.2 \times 18.2 \text{ nm}^2$ ,  $V_T = 739 \text{ mV}$ ,  $i_T = 21 \text{ pA}$ . The unit cell is indicated by a red rhombus ( $a = (2.88 \pm 0.1) \text{ nm}$ ,  $b = (2.97 \pm 0.2) \text{ nm}$ ,  $\alpha = (66.3 \pm 4)^\circ$ ). The main crystallographic directions of the underlying HOPG lattice are marked by the three red lines. b) Corresponding symmetrised correlation-averaged image of the STM image ( $5.88 \times 5.88 \text{ nm}^2$ ). A superlattice of brighter spots is evidenced in red with this colour code. c) Schematic representation of the proposed packing model. The superlattice of brighter spots is shown in green. It is likely to be related to the contrast of the methyl groups pointing out of the plane. d) Side view of  $(S)-(M)-(S')-(M')-(S'')-(M'')$ -**5** after geometry optimisation in the presence of an HOPG model surface with methyl and methoxy groups pointing out of the plane.

(Figure 3). STM evidences that  $(S)-(M)-(S')-(M')-(S'')-(M'')$ -**5** forms a honeycomb structure reminiscent of what has been reported for other large aromatic  $C_3$  symmetrical molecules.<sup>[29–31]</sup> Each hexagonal pattern of the honeycomb structure is formed by six spots with a triangular shape (see red triangles on Figure 3a). Each spot with a triangular shape is composed of three bright spots. The dimensions of one bright spot corresponds to the calculated dimensions of a single motor unit; therefore, we conclude that a single triangle composed of three bright spots corresponds to one molecular motor trimer **5**. The central phenyl core is not visible and within a single molecule the three motor units have a different shape and contrast (Figure 3b).<sup>[32]</sup> This might be a consequence of different conformations of motor parts within a trimer molecule or a consequence of their physisorption on different binding sites of HOPG.<sup>[33]</sup> Upon close inspection of the hexagonal pattern, it appears that the edge of a triangle representing a molecule is not pointing toward the centre of a hexagon, thus forming a chiral array characterised by a clockwise rotational symmetry (Figure 3a,b).<sup>[34]</sup> Analysis of the orientation of the molecular pattern reveals that it forms an average angle of  $\theta = (15.6 \pm 5)^\circ$  with respect to the underlying graphite lattice (the main axis of the HOPG lattice are schematically represented in Figure 3a). Due to the variation of the contrast and shape of individual motor units this angle varies for the triangles forming one hexagon, which induces a large standard deviation. The average angle is similar to the angle ( $18^\circ$ ) between the arms of 1,3,5-triethynylbenzene-based scaffold and the axis between the centre of the fluorenyl moiety and the central benzene ring. Consequently, we can reasonably infer that the triethynylbenzene-based scaffold follows the symmetry and orientation of the underlying graphite. We also assume

that the molecule adsorbs exclusively through one side, which is flat and allows all aromatic parts to interact with the surface (Figure 3d). The methyl and methoxy groups are protruding out of the plane of the molecule on the opposite side. Based on these experimental observations, a tentative packing model is suggested (Figure 3c). On this model, the methyl groups that are pointing out from the surface are shown in green. Since they have the highest physical height, it is expected that the STM signal from the aromatic parts surrounding the empty voids is negligible compared with the contribution of these methyl groups. Therefore, the apparent size of the voids is larger than the empty spaces

of the model: the diameter of the apparent voids on the STM image corresponds to the diameter of the voids on the model as delimited by the methyl groups. Due to the specific packing, the asymmetry of the trimer is expressed on two levels: 1) at the molecular level, as a result of the orientation of each triangular-shaped molecule with respect to graphite, determined by the chirality of the molecule, and 2) at the supramolecular level, as a result of the clockwise or anticlockwise rotational symmetry of the hexagonal pattern. By using enantiomerically pure  $(S)-(M)-(S')-(M')-(S'')-(M'')$ -**5**, only domains with clockwise orientation have been observed.

It is remarkable that large spots are uncovered by **5** in the centre of the hexagon, which is thermodynamically not favoured because of the low surface coverage. Such empty voids were recently observed in systems in which strong and highly directional intermolecular interactions are present.<sup>[35]</sup> In the case of **5**, only weak van der Waals interactions can be established between molecules. When a mixture of diastereoisomers of **5** is deposited on graphite, a self-assembled monolayer is also formed, but with a drastically different structure (see Figure S3 in the Supporting Information). Therefore, the formation of a “low” density packing containing empty voids is attributed to chiral self-recognition between the helically shaped motor units.<sup>[36,37]</sup>

In conclusion, we have developed a new ultrafast molecular motor that contains an aryl bromide moiety for its incorporation into more complex systems by Sonogashira coupling. Motor **4** is, in principle, capable of  $3.3 \times 10^3$  rotations per second at room temperature.<sup>[38]</sup> Molecular motor trimer **5** was found to form organised arrays of molecules by self-assembly at the phenyloctane/HOPG interface. The molecules pack in a honeycomb lattice. In the monolayer the

chirality of the molecule was expressed on the molecular as well as on the supramolecular level. The effect of irradiation on the monolayer dynamics is currently being investigated.

### Acknowledgements

The authors thank NanoNed and The Netherlands Organization for Scientific Research (NWO-CW) for financial support, in particular with a VENI grant (N.K.).

**Keywords:** chirality • molecular devices • nanostructures • photochemistry • scanning probe microscopy

- [1] *Molecular Motors* (Ed.: M. Schliwa), Wiley-VCH, Weinheim, **2003**.
- [2] M. G. L. van den Heuvel, C. Dekker, *Science* **2007**, *317*, 333–336.
- [3] *Molecular Machines and Motors, Struct. Bond. Vol. 99* (Ed.: J.-P. Sauvage), **2001**.
- [4] *Molecular Devices and Machines: A journey into the nanoworld* (Eds.: V. Balzani, M. Venturi, A. Credi), Wiley-VCH, Weinheim, **2006**.
- [5] V. Balzani, A. Credi, F. M. Raymo, J. F. Stoddart, *Angew. Chem.* **2000**, *112*, 3484–3530; *Angew. Chem. Int. Ed.* **2000**, *39*, 3348–3391.
- [6] K. Kinbara, T. Aida, *Chem. Rev.* **2005**, *105*, 1377–1400.
- [7] W. R. Browne, B. L. Feringa, *Nat. Nanotechnol.* **2006**, *1*, 25–35.
- [8] D. A. Leigh, F. Zerbetto, E. R. Kay, *Angew. Chem.* **2007**, *119*, 72–196; *Angew. Chem. Int. Ed.* **2007**, *46*, 72–191.
- [9] C. Dri, M. V. Peters, J. Schwarz, S. Hecht, L. Grill, *Nat. Nanotechnol.* **2008**, *3*, 649–653.
- [10] J. K. Gimzewski, C. Joachim, R. R. Schlittler, V. Langlais, H. Tang, I. Johansson, *Science* **1998**, *281*, 531–533.
- [11] N. Katsonis, M. Lubomska, M. M. Pollard, B. L. Feringa, P. Rudolf, *Prog. Surf. Sci.* **2007**, *82*, 407–434, and references therein.
- [12] N. Katsonis, T. Kudernac, M. Walko, S. J. van der Molen, B. J. van Wees, B. L. Feringa, *Adv. Mater.* **2006**, *18*, 1397–1400.
- [13] N. Koumura, R. W. J. Zijlstra, R. A. van Delden, N. Harada, B. L. Feringa, *Nature* **1999**, *401*, 152–155.
- [14] J. Vicario, A. Meetsma, B. L. Feringa, *Chem. Commun.* **2005**, 5910–5912.
- [15] G. S. Kottas, L. I. Clarke, D. Horinek, J. Michl, *Chem. Rev.* **2005**, *105*, 1281–1376.
- [16] M. M. Pollard, M. Klok, D. Pijper, B. L. Feringa, *Adv. Funct. Mater.* **2007**, *17*, 718–729.
- [17] M. Klok, N. Boyle, M. T. Pryce, A. Meetsma, W. R. Browne, B. L. Feringa, *J. Am. Chem. Soc.* **2008**, *130*, 10484–10485.
- [18] R. A. van Delden, M. K. J. ter Wiel, M. M. Pollard, J. Vicario, N. Koumura, B. L. Feringa, *Nature* **2005**, *437*, 1337–1340.
- [19] M. M. Pollard, M. Lubomska, P. Rudolf, B. L. Feringa, *Angew. Chem.* **2007**, *119*, 1300–1302; *Angew. Chem. Int. Ed.* **2007**, *46*, 1278–1280.
- [20] J.-F. Morin, Y. Shirai, J. M. Tour, *Org. Lett.* **2006**, *8*, 1713–1716.
- [21] Y. Shirai, A. J. Osgood, Y. Zhao, Y. Yao, L. Saudan, H. Yang, C. Yu-Hung, L. B. Alemany, T. Sasaki, J.-F. Morin, J. M. Guerrero, K. F. Kelly, J. M. Tour, *J. Am. Chem. Soc.* **2006**, *128*, 4854–4864.
- [22] M. M. Pollard, A. Meetsma, B. L. Feringa, *Org. Biomol. Chem.* **2008**, *6*, 507–512.
- [23] D. H. R. Barton, B. J. Willis, *J. Chem. Soc. Perkin Trans. 1* **1972**, *3*, 305–310.
- [24] J. Buter, S. Wassenaar, R. M. Kellogg, *J. Org. Chem.* **1972**, *37*, 4045–4060.
- [25] T. Hundertmark, A. F. Littke, S. L. Buchwald, G. C. Fu, *Org. Lett.* **2000**, *2*, 1729–1731.
- [26] J. Vicario, M. Walko, A. Meetsma, B. L. Feringa, *J. Am. Chem. Soc.* **2006**, *128*, 5127–5135.
- [27] For our other molecular motors, unidirectionality of the rotation was proven by following the rotation with <sup>1</sup>H NMR spectroscopy. However, no deuterated solvents in which **5** is sufficiently soluble at 150 K were available to us.
- [28] E. Fischer, *J. Phys. Chem.* **1967**, *71*, 3704–3706.
- [29] S. Furukawa, H. Uji-i, K. Tahara, T. Ichikawa, M. Sonoda, F. C. De Schryver, Y. Tobe, S. De Feyter, *J. Am. Chem. Soc.* **2006**, *128*, 3502–3503.
- [30] X. Feng, J. Wu, M. Ai, W. Pisula, L. Zhi, J. P. Rabe, K. Müllen, *Angew. Chem.* **2007**, *119*, 3093–3096; *Angew. Chem. Int. Ed.* **2007**, *46*, 3033–3036.
- [31] M.-C. Blüm, M. Pivetta, F. Patthey, W.-D. Schneider, *Phys. Rev. B* **2006**, *73*, 195409.
- [32] The superlattice of bright spots is visible in the STM image (Figure 3a). However, it is better highlighted by the colour code in Figure 3b, in which brighter spots belonging to the superlattice appear red. These spots are spaced approximately (1.2 ± 0.2) nm apart. Their possible origin is represented in Figure 3c (methyl groups pointing out of the plane).
- [33] Asymmetry of the tip can be ruled out because the contrast pattern is not altered for two different orientations of the trimer with respect to the scanning direction.
- [34] F. Charra, J. Cousty, *Phys. Rev. Lett.* **1998**, *80*, 1682–1685.
- [35] T. Kudernac, S. Lei, J. A. A. W. Elemans, S. De Feyter, *Chem. Soc. Rev.* **2009**, DOI: 10.1039/b708902n.
- [36] R. Fasel, M. Parschau, K.-H. Ernst, *Nature* **2006**, *439*, 449–452.
- [37] N. Katsonis, A. Minoia, T. Kudernac, T. Mutai, H. Xu, H. Uji-i, R. Lazzaroni, S. De Feyter, B. L. Feringa, *J. Am. Chem. Soc.* **2008**, *130*, 386–387.
- [38] This number is based on the rate of the thermal step ( $k = 9500 \text{ s}^{-1}$ ), in combination with the position of the photoequilibrium (30:70 in favour of the unstable isomer), divided by two (because two thermal conversions are needed to fulfil a complete rotation):  $(9500 \times 0.7)/2$ .

Received: December 23, 2008  
Published online: February 13, 2009